Received: 30 July 2021 | Revised: 1 November 2021 | Accepted: 30 November 2021

DOI: 10.1002/hbm.25741

RESEARCH ARTICLE

WILEY

Olfactory loss and brain connectivity after COVID-19

Fabrizio Esposito[1] | **Mario Cirillo**[1] | **Rosa De Micco**[1] | **Giuseppina Caiazzo**[1] | **Mattia Siciliano**[1] | **Andrea Gerardo Russo**[2] | **Caterina Monari**[3] | **Nicola Coppola**[3] | **Gioacchino Tedeschi**[1] | **Alessandro Tessitore**[1]

[1]Department of Advanced Medical and Surgical Sciences, University of Campania "Luigi Vanvitelli", Naples, Italy

[2]Department of Medicine, Surgery and Dentistry, "Scuola Medica Salernitana," University of Salerno, Baronissi (Salerno), Italy

[3]Department of Mental and Physical Health and Public Medicine, University of Campania "Luigi Vanvitelli", Naples, Italy

Correspondence
Fabrizio Esposito, Department of Advanced Medical and Surgical Sciences University of Campania "Luigi Vanvitelli" Piazza Luigi Miraglia, 2, Naples 80138, Italy.
Email: fabrizio.esposito@unicampania.it

Abstract

To address the impact of COVID-19 olfactory loss on the brain, we analyzed the neural connectivity of the central olfactory system in recently SARS-CoV-2 infected subjects with persisting olfactory impairment (hyposmia). Twenty-seven previously SARS-CoV-2 infected subjects (10 males, mean age ± *SD* 40.0 ± 7.6 years) with clinically confirmed COVID-19 related hyposmia, and eighteen healthy, never SARS-CoV-2 infected, normosmic subjects (6 males, mean age ± *SD* 36.0 ± 7.1 years), were recruited in a 3 Tesla MRI study including high angular resolution diffusion and resting-state functional MRI acquisitions. Specialized metrics of structural and functional connectivity were derived from a standard parcellation of olfactory brain areas and a previously validated graph-theoretic model of the human olfactory functional network. These metrics were compared between groups and correlated to a clinical index of olfactory impairment. On the scanning day, all subjects were virus-free and cognitively unimpaired. Compared to control, both structural and functional connectivity metrics were found significantly increased in previously SARS-CoV-2 infected subjects. Greater residual olfactory impairment was associated with more segregated processing within regions more functionally connected to the anterior piriform cortex. An increased neural connectivity within the olfactory cortex was associated with a recent SARS-CoV-2 infection when the olfactory loss was a residual COVID-19 symptom. The functional connectivity of the anterior piriform cortex, the largest cortical recipient of afferent fibers from the olfactory bulb, accounted for the inter-individual variability in the sensory impairment. Albeit preliminary, these findings could feature a characteristic brain connectivity response in the presence of COVID-19 related residual hyposmia.

KEYWORDS
anosmia, brain connectivity, COVID-19, hyposmia, olfactory network

1 | INTRODUCTION

A number of neurological manifestations suggests the involvement of the central nervous system (CNS) in COVID-19 even though the underlying pathophysiological mechanisms remain a key knowledge gap (Koralnik & Tyler, 2020). Among these, olfactory sensory dysfunction (i.e., hyposmia or complete anosmia) is reported in both acute and postacute phases of the disease (Lechien et al., 2020; Sedaghat, Gengler, & Speth, 2020) and even 6 months after resolution of COVID-19 (Boscolo-Rizzo et al., 2021). As systematic objective olfactory tests would likely reveal hyposmia in at least 80% of COVID-19 patients (Hornuss et al., 2020), the olfactory impairment has become a clinical hallmark of COVID-19 (Lechien et al., 2020; Miller & Englund, 2020).

The prevalence of olfactory loss in COVID-19 individuals has been linked to recent evidence of SARS-CoV-2 crossing the neural-mucosal interface in the olfactory mucosa and affecting the olfactory and sensory nerve endings (Meinhardt et al., 2021), albeit other potential entry routes of SARS-CoV-2 (e.g., via crossing of blood brain barrier or infiltration of infected immune cells) are currently hypothesized (Iadecola, Anrather, & Kamel, 2020). Thereby, assuming that retrograde transmission via olfactory sensory neurons contributes to SARS-CoV-2 neurotropism, making olfactory symptoms more likely to occur in humans, it could be hypothesized that the early (sensory) cortical areas of the olfactory brain network, and specifically the piriform cortex (Roesch, Stalnaker, & Schoenbaum, 2006), would be also affected by, or even neuroplastically responding to, the recent SARS-Cov-2 infection. This mechanism would possibly explain the persisting olfactory impairment, especially in the absence of visible injury along the peripheral olfactory pathway (Eliezer et al., 2020). Indeed, morphometric indices of brain atrophy and axon integrity were mostly found increased in the olfactory areas of recovered COVID-19 patients (compared to healthy volunteers), suggesting that neurogenesis (or other forms of functional compensation) within the CNS might have occurred because of SAR-CoV-2 entering the brain via the olfactory bulb (Lu et al., 2020). On the other hand, a recent PET study (Niesen et al., 2021) on COVID-19 patients with (sudden) olfactory loss, half of which exhibiting bilateral obstructions of the olfactory clefts, only reported subtle and inconsistent (i.e., both increases and decreases) cerebral changes, albeit these were associated with the degree of olfactory impairment.

To possibly gain more specific insight on the early neurosensory impact of COVID-19 hyposmia, here we performed a multi-modal (i.e., structural and functional) neural connectivity analysis of the central olfactory system, using advanced 3 Tesla MRI data. To minimize the confounding effects from other COVID-19 related manifestations, we only recruited previously SARS-CoV-2 infected middle-age subjects, during the early stage of their recovery (i.e., not more than 3 weeks after returning virus-free), with no history of olfactory disturbances before, and referring persisting olfactory impairment after, a noncritical COVID-19 course (World Health Organization, 2020). Moreover, we hypothesized that the structural connectivity of the entire olfactory cortex, and specifically the local functional connectivity of the anterior piriform cortex (APC), that is, the putative largest cortical recipient of direct afferent fibers from the olfactory bulb (Roesch et al., 2006), could be selectively altered in previously SARS-Cov-2 infected hyposmic subjects and eventually correlated with the degree of residual olfactory impairment.

On these premises, our brain connectivity analysis was organized in two stages: First, starting from high angular resolution diffusion imaging MRI data and the widely used automated anatomic labeling (AAL3) (Rolls, Huang, Lin, Feng, & Joliot, 2020) template, we performed a *classification target* tractography (Theisen et al., 2017) of the olfactory cortex. In this way, we derived a morphology-independent structural connectivity index (Tschentscher, Ruisinger, Blank, Díaz, & von Kriegstein, 2019) expressing the log-normalized amount of white matter fibers emerging from the olfactory cortex AAL3 parcel (encompassing the entire piriform cortex and including the olfactory tubercle [Tzourio-Mazoyer et al., 2002]), that we specified as *source* region, and reaching *any* of the other (primary or putative secondary) olfactory cortical areas (see Han, Zang, et al., 2019 for review), that we specified as *target* regions. Second, starting from resting-state fMRI data, we applied a detailed 22-region graph model of the human olfactory functional network (Arnold et al., 2020) to directly zoom into the local functional connectivity of the earliest sensory node of the olfactory cortex, that is, the APC. This model, albeit covering the right hemisphere only, was previously validated on a very large cohort ($n = 812$) of normative subjects in combination with accurate olfactory performance measurements from an independent sample ($n = 33$) (Arnold et al., 2020). As this graph exhibited strong *small-world* properties, presumably in support of both specialized and integrative functions of olfaction, we extracted four *small-world* graph-theoretic metrics (Rubinov & Sporns, 2010) to assess the local functional connectivity of the APC node to the entire olfactory brain network: the *degree*, that is, the discrete number of active APC connections, the *strength*, that is, the functional connectivity weighted sum of all active APC connections, the *local efficiency*, that is, the amount of information transfer within APC neighborhoods, and the *clustering coefficient*, that is, the level of functional segregation of the network around the APC node.

2 | MATERIALS AND METHODS

2.1 | Participants

Twenty-seven subjects (10 males, mean age ± $SD = 40.0 \pm 7.6$ years, age range 27–61) with previous SARS-CoV2 infection (COV+) as revealed by real-time polymerase chain reaction (PCR) for SARS-CoV2 RNA, and eighteen healthy control subjects (6 males, mean age ± $SD = 36.0 \pm 7.1$ years, age range 28–61) with no history of previous SARS-CoV-2 infection (COV−) and normal olfaction, were consecutively recruited for the study from the geographical area of Naples (Italy) between April and December 2020.

Participation requests and clinical interviews to candidate participants were made by medical doctors from the local clinics. The subjects' enrollment in the research was inclusive of all persons, without

limitations by sex or gender, race or ethnicity, or age, other than as scientifically justified and specified in the following inclusion and exclusion criteria.

Subjects between 25 and 65 years of age were considered eligible for the study. Exclusion criteria for the COV+ group included: history of critical COVID-19 (according to WHO guidance (World Health Organization, 2020)), persisting COVID-19 neurological symptoms other than olfactory loss (e.g., memory loss, headache, isolated dysgeusia or ageusia, etc.), pre-existing (i.e., preinfection) olfactory dysfunction (e.g., due to head trauma, congenital olfactory dysfunction, nasal surgery, etc.), history of neurological or psychiatric disorders (before or after infection), and general contraindication to MRI. Exclusion criteria for the COV− group included (pre-existing) olfactory dysfunction, history of neurological, or psychiatric disorders and general contraindication to MRI.

According to WHO classification, the clinical course of COV+ subjects was mild in 20 cases, moderate in 1 case and severe in 6 cases. According to clinical history, the duration of general COVID-19 symptoms in COV+ subjects ranged between 0 (i.e., no symptoms other than olfactory disturbances) and 21 days (9.4 ± 6.6 days, excluding olfactory disturbances). The period of infection, estimated as the time between the first positive real-time PCR and the second consecutive negative real-time PCR, ranged between 10 and 76 days (31.8 ± 21.0 days).

On the scanning day, all COV+ and COV− subjects had recently (13.0 ± 7.4 days, range 1–21 days) undergone a real-time PCR confirming that they were virus-free on the scanning day. All COV− subjects had also received antibody testing to exclude asymptomatic infection. None of the COV− subjects developed clinical COVID-19 symptoms or reported olfactory dysfunction within the subsequent 3 weeks. On the same day, 24/27 COV+ subjects subjectively referred to be hyposmic (duration of olfactory symptoms: 36.4 ± 27.5, range 11–89 days), six of which (6/24) subjectively reported minor hypogeusia in addition to hyposmia. 1/24 subjects experienced parosmia and 3/24 subjects experienced phantosmia. While none of the subjects reported isolated ageusia, dysgeusia, or hypogeusia, all 27 COV+ subjects were eventually confirmed as anosmic, hyposmic, or normosmic based on the functional assessment (see Section 2.2).

All subjects had normal (or corrected-to-normal) vision and hearing and were right-handed and free from global cognitive impairment since all of them scored higher than the age- and education-adjusted Italian cut-off score of Montreal Cognitive Assessment (MoCA; Santangelo et al., 2015).

The study was ethically approved by the Institutional Review Board of the University of Campania "L. Vanvitelli" (Protocol nr. 0008735). A written informed consent was obtained from all subjects participating in the study.

2.2 | Olfactory functional assessment

All subjects underwent a clinical olfactory functional assessment via the Sniffin' Sticks Screening test (Kobal et al., 1996) prior to MRI scanning. This test has been validated in Italian subjects (Eibenstein et al., 2005) and includes 12 sticks containing everyday odors: orange, leather, cinnamon, peppermint, banana, lemon, liquorice, coffee, cloves, pineapple, rose, and fish. The stick is positioned 2 cm from the nose and presented for 3–4 s to be sniffed by the subject. Each stick is presented after an interval of at least 30 s from the others. As the Sniffin' Sticks Screening test is a multiple-forced choice test, the subject is asked to necessarily choose one of the four answers presented in a list, for each odorant. The correct answers were added together to produce a score between 0 and 12.

2.3 | MRI image acquisition

MRI was performed on a 3 Tesla scanner (Discovery MR750, General Electric, USA) equipped with a 32-channel receive-only head–neck coil. The imaging protocol included:

1. Conventional 2D and 3D T2-weighted sequences in the axial plane and a 2D T2-weighted sequence in the coronal plane (25 slices, pixel size $= 0.4 \times 0.4 \times 2$ mm, no gap) covering the anterior and middle segments, for radiological assessment.
2. 3D T1-weighted inversion recovery fast spoiled gradient recalled echo (3D-IR-FSPGR) with sagittal reconstruction (TR = 6,912 ms, IT = 650 ms, TE = 2.996 ms, flip angle = 9°, voxel size $= 1 \times 1 \times 1$ mm) for high resolution anatomical reference.
3. Diffusion MRI: 2D diffusion-weighted spin-echo echo-planar imaging series with axial orientation (66 slices, TR = 7,000 ms, TE = 75 ms, isotropic voxel size 2.0 mm, 5 unweighted volumes for off-line motion-correction, 64 noncollinear isotropically distributed gradient directions with b-value = 2,000 s/mm^2). Two additional series with opposite polarity of the phase encoding direction were acquired for distortion correction.
4. Resting-state fMRI: 2D T2*-weighted gradient-echo echo-planar imaging series with oblique slab orientation (44 slices, TR = 2000 ms, TE = 30 ms, voxel size $2.25 \times 2.25 \times 3$ mm^3, number of volumes 300). Slices were tilted at approximately −30° with respect to the anterior commissure–posterior commissure line to reduce the distortion and improve the signal-to-noise ratio in the olfactory and orbito-frontal cortex (OFC) (Deichmann, Gottfried, Hutton, & Turner, 2003).

All exams were performed during the morning between 9 and 11 a.m. and all subjects were instructed to stay motionless and awake during scanning. Prior to the resting-state fMRI scan, the subjects were reminded via headphones to remain motionless and awake and to keep their eyes closed for the next 10 min.

2.4 | Radiological assessment

For each subject, conventional T2-weighted MRI images were examined with the OSIRIX DICOM viewer (https://www.osirix-viewer.com)

by an author neuroradiologist (MC) with 15 years of experience in head and neck imaging, blinded to the clinical data.

Volumes of the right and left olfactory bulbs were estimated by manually contouring on coronal 2D and axial 3D T2-weighted images using a standardized protocol (Buschhüter et al., 2008). The possible obstruction of the olfactory clefts was visually assessed on 2D coronal T2-weighed images. Presence of obstruction of the space between the cribriform plate, the nasal septum and the upper and middle turbinates was eventually considered as a pathological finding (Eliezer et al., 2020).

White matter hyperintensities were assessed on axial FLAIR images and rated according to the Age-Related White Matter Change and Fazekas scales (i.e., standard 4-point scales for assessing periventricular lesions and deep white matter hyperintensities; Fazekas, Chawluk, Alavi, Hurtig, & Zimmerman, 1987; Wahlund et al., 2001).

2.5 | Structural connectivity analysis

Structural connectivity metrics were derived from diffusion MRI (dMRI) image data which were processed with FSL (https://www.fmrib.ox.ac.uk/fsl) using standard procedures (Jenkinson, Beckmann, Behrens, Woolrich, & Smith, 2012). Data preprocessing included brain extraction, echo-planar image unwarping, eddy current distortion and motion correction and image registration and normalization to standard MNI space.

The left and right olfactory cortex were separately used as seed regions for MRI tractography based on the AAL3 (Rolls et al., 2020; Tzourio-Mazoyer et al., 2002) anatomical template. As target regions, we included all brain regions collecting potential connections from the piriform cortex (see Han, Zang, et al., 2019 for a recent review), ranging from other primary subcortical (e.g., amygdala) and cortical (e.g., entorhinal cortex) to all putative secondary cortical (e.g., OFC, insula, and anterior cingulate cortex) olfactory regions. We also included additional AAL3 parcels contributing one (or more) expected peaks of functional activation in response to a hypothetical contrast "odor stimulus versus baseline" according to a previous meta-analysis of 45 functional neuroimaging studies of olfaction (Seubert, Freiherr, Djordjevic, & Lundström, 2013).

Each AAL3 region in standard MNI space was back-transformed to native diffusion space for each individual subject. For each seed, the following 16 ipsilateral target masks were created: Anterior cingulate cortex pregenual (ACCpre), Anterior cingulate cortex subgenual (ACCsub), Anterior cingulate cortex supracollasal (ACCsup), Amygdala, Caudate nucleus, Hippocampus, Nucleus Accumbens (NAcc), nucleus Pallidum, ParaHippocampal gyrus, Putamen, Anterior orbital gyrus (OFCant), Lateral orbital gyrus (OFClat), Medial orbital gyrus (OFCmed), Posterior orbital gyrus (OFCpost), Insula and Thalamus.

Probabilistic tractography was performed in native (diffusion) space using the FSL program "Probtrackx2" with the "classification target" option enabled and default settings (5,000 streamlines/voxel). An exclusion mask for the contralateral hemisphere was specified for each seed. In this way, starting from the fiber distribution estimates at each voxel, as obtained via the FSL program "BEDPOSTX," the strength and the most likely location of a pathway between the seed and each target area was calculated, resulting in 16 tractographic maps (one per each target region) where only streamlines that propagated to a specific target mask were counted. Because the number of streamlines for each seed-target pair is dependent on the size of the seed region, a normalized connectivity index (Tschentscher et al., 2019) was calculated as $\frac{\log_{10} S_t}{\log_{10} 5{,}000 \cdot V_s}$ (where S_t is the total number of streamlines successfully propagated to the target region and V_s is the total number of voxels in the seed region).

2.6 | Functional connectivity analysis

2.6.1 | Resting-state fMRI data preprocessing

Functional connectivity metrics were derived from resting-state fMRI data which were preprocessed with BrainVoyager 22.0 (Brain Innovation B.V., www.brainvoyager.com; Goebel, 2012) using standard procedures for slice scan timing correction, 3D rigid head motion correction, temporal filtering, image registration and brain normalization to standard MNI space. The log files with motion parameter estimates (three translation and three rotation values per time point) were both reviewed (for quality insurance) and later used for high-order motion correction of the voxel time-series. At this stage, subjects exhibiting head translations >3 mm and/or head rotations >3° would be excluded from the subsequent analyses. To reduce linear and nonlinear trends in the time courses, each rs-fMRI time series was temporally filtered in the frequency domain using a high-pass filter with a cut-off set to 0.008 Hz. Within the spatial normalization step, all volumes were resampled to isotropic voxel size (2 mm) using 3D sinc interpolation and spatially smoothed with an isotropic Gaussian kernel (full width half maximum 6 mm).

Prior to the functional connectivity analysis, the residual effects of head motion (including residual motion-related spikes) and physiological nuisance signals (from respiratory and cardiac sources) on the variance of resting-state fMRI data, were filtered out via linear regression (Friston, Williams, Howard, Frackowiak, & Turner, 1996; Satterthwaite et al., 2012; Satterthwaite, Wolf, et al., 2013). To this purpose, a linear regression model was applied to each voxel time-course in Matlab (The Mathworks, Inc., www.mathworks.com), using Neuroelf (www.neuroelf.org) access functions to import the initial data set and running a custom Matlab script to (iteratively) apply the Matlab function "regress" and to export the final 4D data set from the model residuals time-courses. The model included 24 motion-related predictors (6 head motion parameter time-series, their first-order derivatives, and the 12 corresponding squared parameter time-series), two physiological noise predictors (the mean regional time-courses from a white matter mask and a cerebrospinal fluid mask, as obtained from the MNI template brain) and a "spike-only" predictor (to capture the variance associated with possible motion-related spikes in the time-series). This last predictor was derived from the instantaneous framewise displacement (FD) (Power et al., 2014; Satterthwaite,

Elliott, et al., 2013), that is, a 300-timepoint vector was initialized to zero at all time points, then, where FD exceeded a threshold of 0.5 mm, the value at that time point, as well as the values at one point before and one and two time points after, were set to one. At this stage, as a further quality insurance criterion, the percentage of spike-corrupted volumes (i.e., FD >0.5 mm) had not to exceed 50% of the time series and the mean FD had not to exceed 0.25 mm (Parkes, Fulcher, Yücel, & Fornito, 2018; Power et al., 2014).

2.6.2 | Functional connectivity network-level analysis

Twenty-two regions of interest (ROI) were considered according to the graph model derived by Arnold et al. (2020) which prescribes placing one or more nodes within each of the following areas: piriform cortex, amygdala, hippocampus, entorhinal, olfactory tubercle, OFC, insula, hippocampus, thalamus, nucleus accumbens, and hypothalamus (Figure 1).

For each node, a spherical ROI was drawn on the MNI template in BrainVoyager. The sphere centers were placed at the centroid coordinates reported in (Arnold et al., 2020). To avoid dependency on ROI size, the radius of the sphere was set to 4 mm (which is the most typical choice for resting-state fMRI studies), resulting in ROI volumes of 268 mm^3 (the mean size of the original ROI parcels being 266 mm^3; Arnold et al., 2020).

ROI-specific time-series were extracted from the preprocessed data in Matlab (The Mathworks, Inc., www.mathworks.com) using Neuroelf (www.neuroelf.org) access functions.

Pearson's correlation coefficients (r) were calculated for each pair of ROI-specific time-series to construct a symmetric 22 × 22 connectivity matrix for each subject. The mean FD was regressed out from the series of r values (across subjects). The overall (absolute) functional connectivity in each subject was then calculated from the mean of all positive r values after setting all negative r values to zero (van den Heuvel et al., 2017) as well as from the mean of all absolute r values (i.e., including negative r values). Both the significantly positive and the significantly negative connections (one-tail one-sample t-test on Fisher z-transformed r values vs. zero, p <.05 Bonferroni corrected across all connections) were counted in each group and the proportions of positive and negative connections in the network were compared between groups using a Fisher's exact test on the resulting 2-by-2 contingency table (with odd ratio and 95% confidence interval).

2D circular graphs and 3D network graphs were generated by group-level averaging of the absolute functional connectivity and interactively displayed in Matlab using the "circularGraph" built-in function and the "BrainNet" viewer toolbox (Xia, Wang, & He, 2013). To display the stronger functional connections in each group, a descriptive threshold (ranging from $r = .10$ to $r = .25$ with a step of .05) was applied to the group-specific average network weights that were significantly positive in each group (one-tail one-sample t-test on Fisher z-transformed r values vs. zero, p <.05 Bonferroni corrected across all connections).

To specifically assess (and compare between groups) the local topological properties of the functional network at the APC node, the maximum number of "active" connections over the entire network (i.e., among all nodes) was equalized across subjects via proportional thresholding (van den Heuvel et al., 2017). Then, the following graph metrics were derived for the APC node using the Brain Connectivity Toolbox (Rubinov & Sporns, 2010): *degree*, *strength*, *local efficiency*, and *clustering coefficient*. To avoid dependency of the results on a specific threshold (Garrison, Scheinost, Finn, Shen, & Constable, 2015), the proportional threshold was varied between 5% (i.e., up to 226/238 most active connections included) and 95% (i.e., up to 11/238 most active connections included) with a step of 5%, and the mean of all threshold-specific metric values was returned. Because functional connectivity networks created from positive and/or

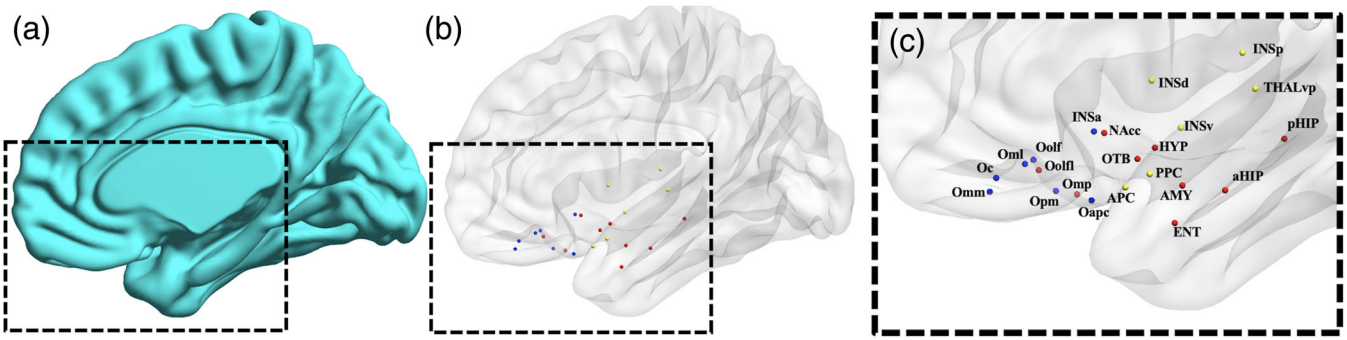

FIGURE 1 Olfactory functional network. (a) Three-dimensional surface of the right brain template (medial view). (b) Three-dimensional glass surface showing the anatomical location and the functional submodule assignment of each node (sensory: yellow, limbic: red, frontal: blue). (c) Zoomed view of the glass surface with node labels: aHIP, anterior hippocampus; AMY, amygdala; APC, anterior piriform cortex; ENT, entorhinal cortex; HYP, hypothalamus; INSa, anterior insula; INSd, dorsal insula; INSp, posterior insula; INSv, ventral insula; Nacc, nucleus accumbens; Oapc, anterior-APC OFC; Oc, central OFC; Oml, medial lateral OFC; Omm, middle medial OFC; Omp, posterior middle OFC; Oolf, olfactory OFC; Oolfl, lateral olfactory OFC; Opm, posterior medial OFC; OTB, olfactory tubercle; pHIP, posterior hippocampus; PPC, posterior piriform cortex; THLvp, ventral posterior thalamus

negative active connections might have different topological properties (see, e.g., Schwarz & McGonigle, 2011), but also considering that the interpretation of negative functional connections is not fully established in the normative literature, the most common approach of analyzing positive functional connections was chosen to determine the metrics of interest for the olfactory functional network. Nonetheless, the results obtained by including both positive and negative connectivity values in the topological analysis are also reported by taking the absolute values of the connectivity prior to thresholding.

2.7 | Statistical analysis

A statistical analysis of MRI-derived measures was performed in Matlab. Two-tailed two-sample *t*-tests and chi-squared tests were performed to compare age and sex proportion between groups. The correction for covariates was performed via linear regression. A two-tailed Wilcoxon rank sum test was performed to compare the medians of Sniffin' test scores between groups.

Two-tailed permutation tests (Good, 2005) were performed (a) to compare the means of MRI-derived (age- and sex-adjusted) measures between two groups using the "permutationTest" function (L. R. Krol, 2021. Via: Matlab Central) and (b) to correlate the (age- and sex-adjusted) Sniffin' test scores to the (age- and sex-adjusted) MRI-derived measures based on Spearman's correlation coefficient (ρ) using the "mult_comp_perm_corr" function (D. Groppe, 2011. Via: Matlab Central). The number of permutations was set to 10,000. For two-sample (comparative) tests, the size of each sample, the effect size (Hedges' g) (*g*) and the *p*-value (*p*) are reported. For one-sample (correlation) tests, the size of the sample, the Spearman's correlation coefficient (ρ) and the *p*-value (*p*) are reported. Beeswarm and box plots and scatter plots were generated to descriptively compare statistical distributions and to display linear correlation trends.

3 | RESULTS

3.1 | Clinical and radiological assessment

On the scanning day, all 27 COV+ subjects failed to correctly identify at least one out of 12 Sniffin' sticks (mean Sniffin' test score ± *SD*: 8.4 ± 2.2, range 2–11), whereas all 18 COV− subjects obtained the maximal score (12/12). The two groups significantly differ in the median Sniffin' test score (median COV+: 9, median COV−: 12, $p < 10^{-8}$). Among COV+ subjects, 5 subjects were anosmic (Sniffin's test score below 7), 18 subjects were hyposmic (Sniffin' test score between 7 and 10) and 4 subjects were normosmic (Sniffiin' test score between 11 and 12) (Hinz et al., 2019). All subjects were cognitively unimpaired (corrected MoCA score >15.5). The two groups did not significantly differ in age ($p = .12$) and sex proportion ($p = .80$).

Conventional MRI displayed no pathological white matter abnormalities and no obstruction of the olfactory clefts in any of the subjects. A slightly reduced volume of the olfactory bulbs was observed in COV+ ($n = 27$) (left: 40.3 ± 8.3 mm^3, right: 41.0 ± 7.6 mm^3), compared to COV− ($n = 18$) (left: 45.4 ± 7.2 mm^3, right: 45.1 ± 7.7 mm^3), subjects, but none of these differences were statistically significant (left: $g = -0.52$, $p = .090$; right: $g = -0.39$, $p = .20$), nor were these measures significantly correlated with the Sniffin' test scores (left: $\rho = -.13$, $p = .52$; right: $\rho = -.14$, $p = .48$).

3.2 | Structural connectivity

The tractography-derived structural connectivity index was significantly higher in COV+ ($n = 27$), compared to COV− ($n = 18$), subjects in the medial OFC subdivision, for both hemispheres (left: $g = 1.18$, $p = .0007$; right: $g = 1.07$, $p = .0009$; both: $p < .05$ after correction for multiple comparisons across all 32 target regions) (Figure 2).

Across all COV+ ($n = 27$) subjects, the olfactory structural connectivity index was not significantly correlated to the Sniffin' test score for any of the target regions, including the medial OFC (left olfactory cortex to medial OFC: $\rho = -.11$, $p = .95$; right olfactory cortex to medial OFC: $\rho = +.24$, $p = .23$).

3.3 | Functional connectivity

Three subjects (2 COV+, 1 COV−) did not successfully complete the full exam protocol with the fMRI scan, thereby the functional connectivity analysis included 25 COV+ subjects (10 males, mean age ± *SD* = 39.6 ± 7.8, mean Sniffin' test score ± *SD* = 8.2 ± 2.2) and 17 COV− subjects (5 males, mean age ± *SD* = 36.2 ± 7.3, Sniffin' test score = 12). The two groups did not significantly differ in age ($p = 0.16$) and sex proportion ($p = 0.48$).

The overall absolute functional connectivity was not significantly different between COV+ and COV− groups, either excluding ($g = -0.0071$, $p = .98$) or not excluding ($g = -0.011$, $p = .97$) negative values from the connectivity matrices (i.e., using absolute values). All significant connections to the APC were found to be positive. When considering signed connectivity values, the overall number of significant positive (negative) connections was respectively 117 (32) for the COV+ group and 151 (40) for the COV− group, corresponding to 51% (14%) and 65% (17%) of all possible network connections (231). The two groups did not significantly differ in the proportions of positive and negative connections (odds ratio: 1.0325, 95% confidence interval: 0.61, 1.74).

Both *degree* and *strength* of the APC functional connectivity were significantly higher (*degree*: $g = 0.73$, $p = .024$; *strength*: $g = 0.68$, $p = .036$; both: $p < .05$) in COV+ ($n = 25$) vs. COV− ($n = 17$) subjects (Figure 3a). Similar trends were observed when including negative connectivity values in the connectivity matrices (*degree*: $g = 0.66$, $p = .041$; *strength*: $g = 0.62$, $p = .055$). Across individual COV+

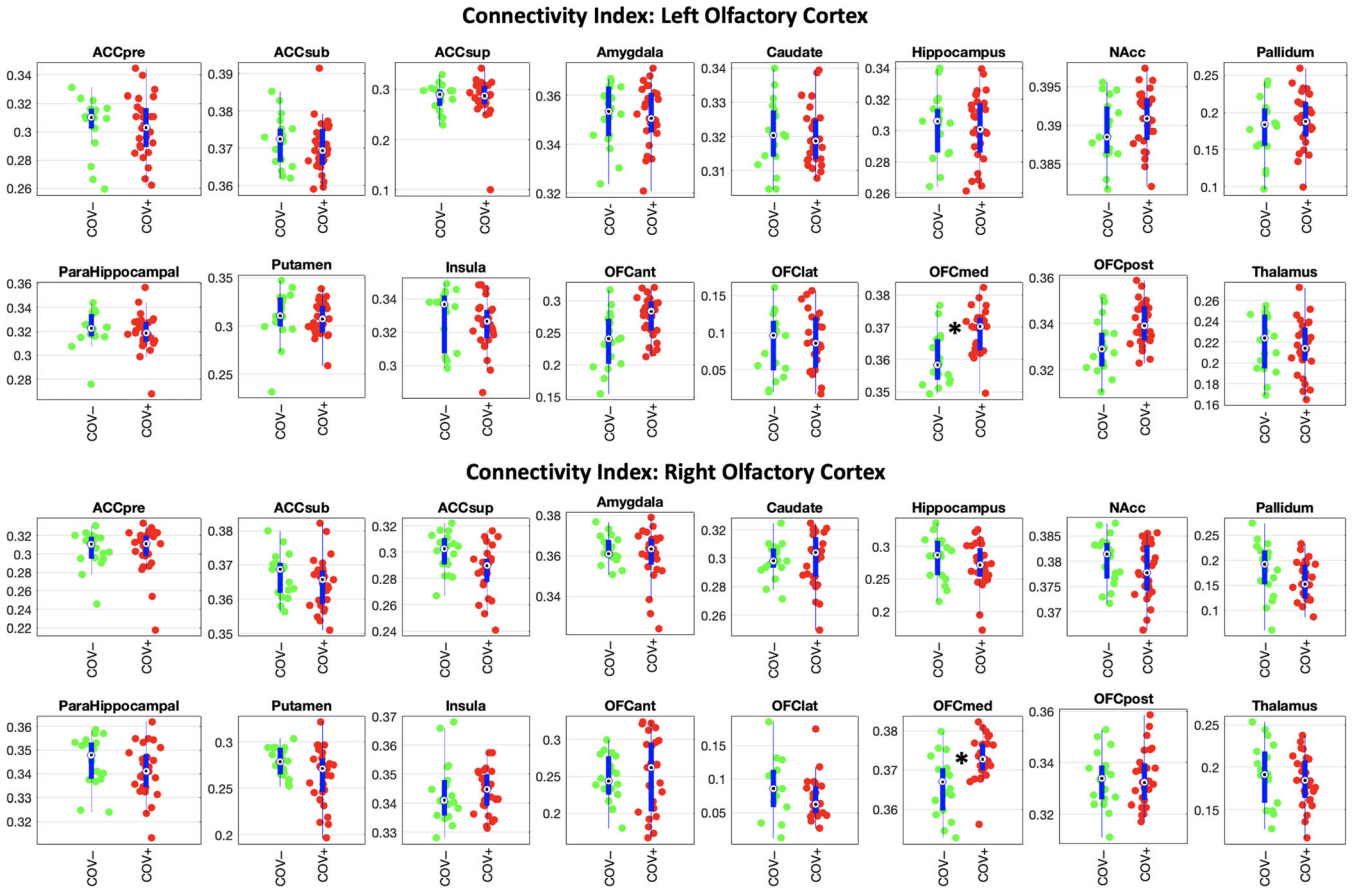

FIGURE 2 Structural connectivity data analysis. Beeswarm and box plots comparing the distributions, the medians, the inter-quartile (IQR, thick blue lines) and extended interquartile (±1.5 IQR, thin blue lines) ranges of the connectivity index, for both source regions (left and right olfactory cortex) and each (ipsilateral) target region (data adjusted for age and sex: COV+ red points, COV− green points). ACC: anterior cingulate cortex (pre: pregenual, sub: subgenual, sup: superior), NAcc: nucleus accumbens, OFC: orbito-frontal cortex (ant: anterior, lat: lateral, med: medial, post: posterior). A star in the plot indicates statistically significant differences between COV+ and COV− groups

subjects ($n = 25$), neither *degree* nor *strength* was significantly correlated to the Sniffin' test score, whether excluding negative values from the connectivity matrices (*degree*: $\rho = .28$, $p = .17$; *strength*: $\rho = -.11$, $p = .59$) (Figure 3b) or not (*degree*: $\rho = .30$, $p = .15$; *strength*: $\rho = -.11$, $p = .62$).

Both *local efficiency* and *clustering coefficient* were not significant different between COV+ ($n = 25$) and COV− ($n = 17$) groups, whether excluding negative values from the connectivity matrices (*local efficiency*: $g = 0.43$, $p = .17$; *clustering coefficient*: $g = 0.31$, $p = .33$) (Figure 3a) or not (*local efficiency*: $g = 0.47$, $p = .14$; *clustering coefficient*: $g = 0.43$, $p = .18$). Across individual COV+ subjects ($n = 25$) both *local efficiency* and *clustering coefficient* were significantly (and inversely) correlated to the Sniffin' test score in COV+ subjects (*local efficiency*: $\rho = -.43$; *clustering coefficient*: $\rho = -.44$; both: $p < .05$) (Figure 3b). Similar correlations were obtained when including negative connectivity values in the connectivity matrices (*local efficiency*: $\rho = -.33$; *clustering coefficient*: $\rho = -.43$) albeit the association was only statistically significant ($p < .05$) for the *clustering coefficient*. Moreover, when additionally correcting (both Sniffin' test scores and connectivity metrics) for the duration of general COVID-19 symptoms, both *local efficiency* and *clustering coefficient* remained significantly (and inversely) correlated with the Sniffin' test scores ($p < .05$). However, when correcting for either the period of infection (estimated from the dates of the first positive PCR and the first negative PCR) or the duration of the olfactory symptoms, both connectivity metrics were not significantly correlated with the Sniffin' test scores ($p > .05$).

The topological differences associated with the functional connectivity effects were visualized using 3D and 2D group-specific graphs showing the active connections.

From the 3D graphs (Figure 4), we note how, at a given absolute threshold of functional connectivity (e.g., $r = .2$ for graph readability), more supra-threshold functional connections occur for the group of COV+ subjects, linking the APC node, not only to the closest sensory nodes along the posterior piriform cortex-APC-OFC axis, but also to additional limbic nodes within primary olfactory areas (olfactory tubercle, amygdala) and to posterior-middle OFC, which, in turn, also appear more inter-connected among themselves. Beyond APC, extra connections can also be noted for the group of COV+ subjects between the (sensory) PPC node and additional limbic nodes

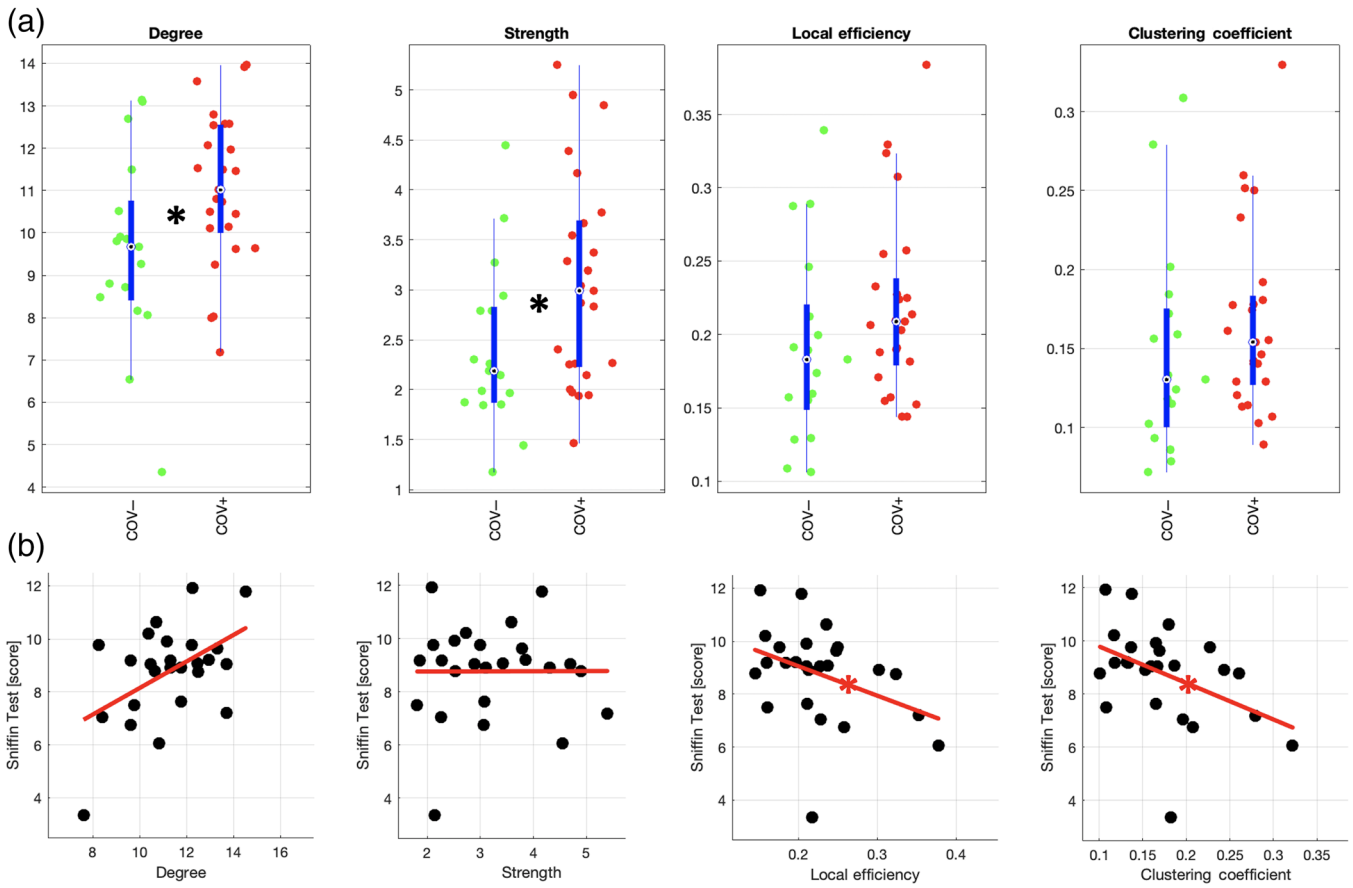

FIGURE 3 Functional connectivity data analysis. (a) Beeswarm and box plots comparing the distributions, the medians, the inter-quartile (IQR, thick blue lines) and extended interquartile (±1.5 IQR, thin blue lines) ranges of degree, strength, local efficiency and clustering coefficient for the APC node (data adjusted for age and sex: COV+ red points, COV− green points). A star in the plot indicates a statistically significant difference between COV+ and COV− groups. (b) Scatter plots with linear trend lines in red displaying the correlation of the same measures with Sniffin scores in COV+ subjects (data adjusted for age and sex: COV+ black points). A star on the line indicates a statistically significant correlation

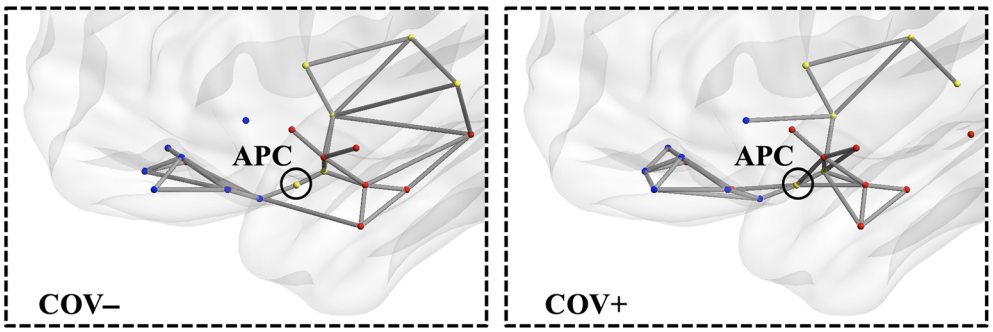

FIGURE 4 Functional connectivity 3D topology. Functional connections traced in gray for COV− (left) and COV+ (right) groups (absolute functional connectivity threshold: Pearson $r = .20$, one-sample t-test on z values >0: $p < .05$, Bonferroni corrected for all possible connections)

(e.g., entorhinal), while it appears there is a lack of functional connectivity in the COV+ group between at least two sensory nodes in the insula (posterior and ventral insula) and two limbic nodes in the hippocampus (anterior and posterior hippocampus). A post hoc comparison of the mean functional connectivity (two sample t-test with signed values) on inter-module connections between COV+ and COV− groups, resulted in a significantly ($p < .05$) increased functional connectivity between PCC and entorhinal and a reduced functional connectivity in three connections between insula and hippocampus nodes.

The 2D circular graphs (Figure 5) particularly highlight the topological effects of a higher degree (i.e., more surviving connections) at various thresholds of absolute functional connectivity (ranging from $r = .10$ to $r = .25$ with step of .05) observed for the APC node in the group of COV+, compared to COV−, subjects. For example, reducing the threshold to $r = .10$ gives additional limbic nodes in the enthorinal cortex and anterior hippocampus and additional frontal nodes in middle and posterior-medial OFC connected to APC for the COV+ group.

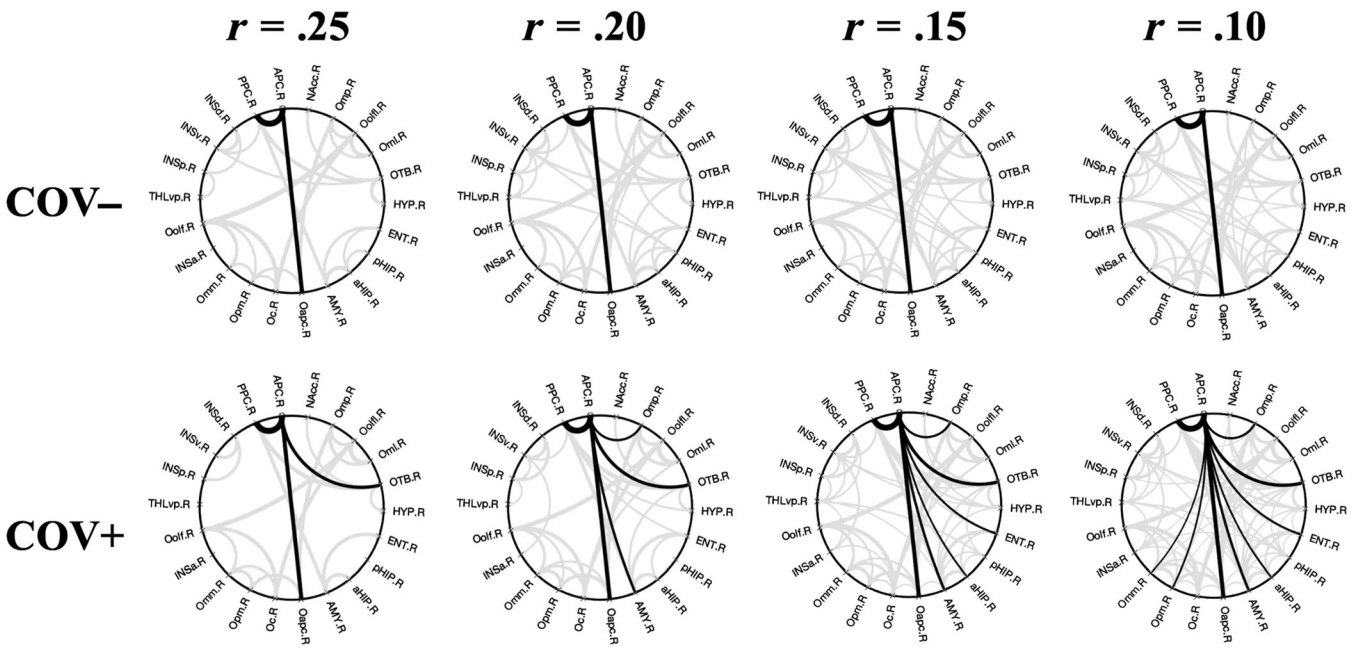

FIGURE 5 Functional connectivity 2D topology. Circular connectograms for COV− (upper row) and COV+ (lower row) groups at multiple thresholds for the absolute functional connectivity (Pearson *r* values: $r = .25$, $r = .20$, $r = .15$, $r = .10$, one-sample *t*-test on *z* values >0: $p < .05$, Bonferroni corrected for all possible connections). Supra-threshold APC connections are traced in black whereas all other connections are traced in gray

4 | DISCUSSION

During the pandemic outbreak, a vast amount of evidence has been accumulating describing the different forms of possible CNS involvement in SARS-CoV-2 infection in relation to the more frequently observed neurological symptoms and their associated radiological and laboratory findings (Paterson et al., 2020). In this study, we explored a possible link between COVID-19 related hyposmia and olfactory brain connectivity. We show how the olfactory brain connectivity of recently SARS-CoV-2 infected hyposmic subjects can be increased (compared to non-SARS-CoV-2 infected normosmic subjects), their residual olfactory loss being associated with more segregated functional connectivity around the APC node of a graph model of the human functional olfactory network.

According to preliminary radiological assessment, we report no edema of the olfactory clefts in any our subjects, suggesting how their possible obstruction, if ever occurred, was fully reverted in COV+ subjects during recovery (Eliezer et al., 2020). Moreover, we found no evidence of systematic alteration in the volumes of the olfactory bulbs, nor these measures significantly explained the clinical variability in the Sniffin' test scores, in COV+ subjects. As we had also considered that humans can have normal olfaction without apparent olfactory bulbs (Weiss et al., 2020), the search for possible neural alterations was extended to the olfactory cortex using advanced MRI methods for brain connectivity analyses.

For the analysis of the olfactory brain connectivity, two different bran parcellations were used, respectively for the dMRI and resting-state fMRI data acquired in the present study. A standard gray matter anatomic parcellation (AAL3) was used to assess the structural integrity of the major bundles connecting the entire olfactory cortex (corresponding to a single extended AAL3 parcel) to all anatomical regions known to be involved in the neural processing of olfactory information processing. While the size and coverage of the AAL3 parcels was well suited for the tractographic analysis of dMRI data, no topological analysis of either structural or functional connectivity was possible on this parcellation, as there is no prior evidence available that the resulting AAL3 sub-parcellation has sufficient small-world properties to justify the estimate of local metrics in a graph model of the olfactory network, nor it would be correct to assume the AAL3 parcels as functionally homogeneous. Instead, a local topological analysis of the APC functional connections was possible using a different parcellation, according to the previous work by Arnold et al. (2020). Besides providing a locally more detailed lay-out of the possible APC connections (e.g., involving multiple distinct parcels in the insular and OFC as well as relatively smaller structures such as the hypothalamus and the olfactory tubercle), the graph model associated with this parcellation has been previous shown to possess strong small-world properties in the context of the human whole-brain connectome (Arnold et al., 2020). However, this functional parcellation was not equally well suited to the structural connectivity analysis as the back-transformation of its parcels to the native space of dMRI data would have produced ROIs of ∼30–35 voxels in total (given the native resolution of 2 mm), with very few voxels at the boundary of the white matter, making the results of the probabilistic tractography unreliable (Catani, Howard, Pajevic, & Jones, 2002; Hagmann et al., 2006).

According to MRI tractography, the structural connectivity from the entire olfactory cortex to the medial OFC, that is, one of the main secondary olfactory functional areas (Tobia, Yang, & Karunanayaka, 2016), was found significantly increased in COV+ hyposmic subjects, compared to age- and sex- matched COV− normosmic subjects. This would be in line with previous morphometric MRI findings (Lu et al., 2020) in COVID-19 patients reporting increased white matter fractional anisotropy, in primary and secondary olfactory tracts (at baseline and 3-month follow-up). However, consistently with this study, we also could provide no evidence of significant association between the structural connectivity of the olfactory cortex and the residual olfactory loss in SARS-CoV-2 infected subjects.

According to a network-level analysis of resting-state fMRI data, the functional connectivity of the APC, that is, the earliest sensory node in a previously validated graph model of the central olfactory functional network in the healthy brain, was found both significantly increased (in terms of *degree* and *strength*) and significantly accounting for the interindividual differences in residual olfactory impairment (in terms of *local efficiency* and *clustering coefficient*), in previously SARS-CoV-2 infected hyposmic subjects. Particularly, greater sensory impairment was positively associated with higher functional segregation at the APC, suggesting that, shortly after COVID-19, an acquired and persisting olfactory loss would be coupled with an excess of specialized sensory processing in regions more densely (functionally) connected to the APC.

This study has two important limitations: First, there was no data available, either concerning the olfactory performance or the neural connectivity of the analyzed COV+ subjects, from the preinfection period. Second, while we could target and verify hyposmia as a frequent, objective and distinctive symptomatic COVID-19 feature in COV+ subjects, we could collect no data from symptom-specific control groups, that is, we could not include recently SARS-CoV-2 infected, and yet perfectly normosmic, subjects, without other neurological manifestations, nor we included a control group with COV− subjects with clinically manifest olfactory loss. These two aspects, together with the limited sample size of the study, imply that the present findings should be taken as preliminary and might still reflect some general effects of olfactory loss rather (or more) than COVID-19 specific effects.

Nonetheless, by taking together the results from two independent neural connectivity analyses of the same subjects, these preliminary findings may generate some new and pathophysiologically relevant hypotheses about the response of the human CNS, either to the recent neuro-invasion of SARS-CoV-2 (Lu et al., 2020) or, more simply, to the persisting olfactory loss, causing a prolonged lack of sensory stimulation to the central olfactory system, in the brain of hyposmic subjects after COVID-19 (Le Bon et al., 2021; Niesen et al., 2021).

Before elaborating such hypotheses, it should be preliminary considered that any of the observed differences might have existed before infection (indicative of a vulnerability), occurred during infection (indicative of a damage) or occurred rapidly after infection (indicative of a recovery), all three scenarios being not mutually exclusive in the generation of the overall pattern. Moreover, it is equally not possible to rule out that the same differences may be due to more general differences in the brain. In fact, while none of the COV+ subjects had neurological symptoms (other than olfactory impairment) on the day of scanning, we are not at all excluding that COV+ subjects may have experienced more diffuse neurological effects during the period of infection which ultimately affected the connectivity of the olfactory regions, as measured on the day of scanning. Particularly, as the functional connectivity analysis was based on resting-state, rather than olfactory task-based, fMRI data, these differences, whether reflecting the olfactory impairment after COVID or not, could still be in principle unrelated to odor responses. In fact, the olfactory regions are not strictly unimodal and no control connectivity analysis was possible here on the visual network (like, e.g., in Arnold et al. (2020)) because the slice acquisition was purposedly tilted to optimize the functional coverage of the orbito-frontal cortex, precluding a whole-brain connectivity analysis.

As a first scenario, assuming that no similar changes would have been (hypothetically) observed before infection, we would provide specific evidence that neurogenesis along the central olfactory pathway, or, possibly, rewiring of the connections from the olfactory cortex, might have rapidly maturated in COV+ hyposmic subjects already after 4 weeks (in average) of infection or 5 weeks (in average) of reduced sensory stimulation. In this case, ascribing these neural effects (only) to a lack of sensory stimulation, already existing since long before SARS-CoV-2 infection, would be strongly against recent evidence that even a lifelong absence of olfactory experience may have a very limited impact on the local functional connectivity of the olfactory cortex (Peter et al., 2021), whereas recently acquired sensory loss has been previously associated with both changed cerebral morphology within core olfactory areas and increase (dynamic) functional connectivity from olfactory cortex to cerebral areas processing multisensory integration (Iravani et al., 2021).

On the other hand, as structural connections are usually more temporally stable than functional connections (Sporns, 2018), in the absence of a robust correlation with the degree of olfactory impairment, it is obviously not possible to rule out that the observed structural connectivity differences between the two groups might have existed already before the infection of COV+ subjects, that is, independently, and in spite of no history, of manifesting olfactory disturbances. This second scenario would imply that the experienced COVID-19 related hyposmia could be itself a sign of increased susceptibility or predisposition to this kind of SARS-CoV-2 neurotropism, whereby the penetration of the virus to the brain via the olfactory pathway would expectedly affect the APC functionality first. Indeed, *local efficiency* and *clustering coefficient*, that we found coupled with olfactory impairment, represent two network characteristics that would expectedly account for the (pathologically insulting) interindividual variability in postinfection olfactory experiences (Arnold et al., 2020). Of note, the correlations between the olfactory impairment and the functional connectivity metrics were robust to the correction for the variable duration of general COVID-19 symptoms (all

extinguished on the day of scanning) albeit they ceased to be significant when correcting (both the clinical scores and the metrics) for the duration of either the estimated period of COVID-19 infection or the experienced olfactory dysfunction (persisting at the day of scanning). Thus, while the coupling between olfactory impairment and functional connectivity was unaffected by the duration of previously experienced general symptoms, it is likely that the degree of olfactory impairment was itself variable in COV+ subjects during the period of infection. However, as the olfactory assessment was only available at the day of scanning, it was not possible to properly account for this other potential source of variability in the data.

Thus, in either case, our findings suggest that the olfactory network mimics a network of cognitive reserve (Stern, 2002), the olfactory loss configuring a sensory proxy of a characteristic COVID-19 reserve of neural plasticity. In support of this interpretation, would be the observation that those infected individuals with greater olfactory loss are also those for whom the olfactory network might have more strongly reacted by functionally insulating the APC node with its closer (more local) connections from other (more distant) nodes. Of note, a rapidly increased functional segregation would be not expected to be coupled to the underlying structural connectivity (Fukushima et al., 2018). Even beyond the APC node, some extra connections were specifically noted for the group of COV+ subjects between the (sensory) PPC node and some limbic nodes (e.g., entorhinal), despite a lack of functional connectivity in the same group between two more distant sensory nodes in the insula (i.e., posterior and ventral insula) and two (limbic) nodes in the hippocampus (i.e., anterior and posterior hippocampus). As it has been previously shown how the right hippocampus activation response to emotional pictures is correlated with the OB size and specifically reduced in dysosmic patients (Han, Hummel, et al., 2019), the observed reduction in the functional connectivity between the hippocampus and the insula in COV+ subjects may suggest that COVID-19 olfactory impairment might have similarly affected the neural processing of nonolfactory information such as, for example, emotional information. In this case, according to the proposed interpretation, the increased connectivity of APC and PPC sensory nodes to other frontal or limbic nodes might be seen as an attempt of the CNS to compensate this damage by remodulating the central olfactory network. However, future task-based fMRI studies, possibly involving both COV+ and COV− subjects with olfactory dysfunction, are needed to confirm such a specific modular re-organization of the olfactory network, after COVID-19.

The concept of neural reserve has been often used to refer to active processes that involve facilitating the flexibility or efficiency of neural networks to compensate for impairments (Stern, 2002). If confirmed by follow-up studies on longer terms, our structural findings would suggest this be an innate characteristic of long-term COVID-19 hyposmic subjects. Thereby, as local efficiency and segregation of the olfactory functional network are deemed critical for accurate olfactory discrimination among normosmic subjects (a proper balance between functional integration and segregation of sensory nodes being essential to limit affective and cognitive influences to olfactory perception; Arnold et al., 2020), the newly observed association of increased COVID-19 related loss of smell with increased local segregation at APC might feature a characteristic neuroprotective response of the CNS.

5 | CONCLUSIONS

In conclusion, while future studies will possibly confirm the current notion of SARS-CoV-2 neurotropism preferentially mediated by the olfactory network (as hypothesized by others), the increased functional segregation of the olfactory network around the APC node, besides calibrating the clinically observable olfactory impairment, might eventually signal a mechanism by which the brain attempts to (at least initially) counteract a more widespread neurological involvement. In this case, the mechanism of infection involving the olfactory route, besides determining the frequently observed olfactory impairment, could stimulate a "self-limiting" response of the CNS, which attempts to compensate other neurological manifestations during, or in the early aftermath of recovery from, SARS-COV-2 infection. Thus, while future brain connectivity studies with larger sample sizes and more specific control groups are needed to confirm or expand these preliminary observations, a longitudinal (follow-up) analysis will be even more necessary to also evaluate the long-term neurological sequelae of COVID-19.

CONFLICT OF INTEREST

The authors declare that they have no conflict of interest.

DATA AVAILABILITY STATEMENT

The conditions of our ethics approval did not permit public archiving of study data. Anonymized data will be shared by request from any qualified investigator from the corresponding author. Access will be granted to named individuals in accordance with ethical conditions governing the reuse of sensitive data. The connectivity matrices (both r and z data, before and after correction for mean framewise displacement) can be downloaded as Matlab (MAT) files from https://osf.io/c8jrq/. Relevant information on the subjects (age, sex, and group) is anonymously provided in the file names.

ORCID

Fabrizio Esposito https://orcid.org/0000-0002-5099-9786
Alessandro Tessitore https://orcid.org/0000-0002-2913-6548

REFERENCES

Arnold, T. C., You, Y., Ding, M., Zuo, X.-N., de Araujo, I., & Li, W. (2020). Functional connectome analyses reveal the human olfactory network organization. *ENeuro*, *7*(4), 1–14. https://doi.org/10.1523/ENEURO.0551-19.2020

Boscolo-Rizzo, P., Menegaldo, A., Fabbris, C., Spinato, G., Borsetto, D., Vaira, L. A., … Hopkins, C. (2021). Six-month psychophysical evaluation of olfactory dysfunction in patients with COVID-19. *Chemical Senses*, *46*, bjab006. https://doi.org/10.1093/chemse/bjab006

Buschhüter, D., Smitka, M., Puschmann, S., Gerber, J. C., Witt, M., Abolmaali, N. D., & Hummel, T. (2008). Correlation between olfactory

bulb volume and olfactory function. *NeuroImage*, *42*(2), 498–502. https://doi.org/10.1016/j.neuroimage.2008.05.004

Catani, M., Howard, R. J., Pajevic, S., & Jones, D. K. (2002). Virtual in vivo interactive dissection of White matter fasciculi in the human brain. *NeuroImage*, *17*(1), 77–94. https://doi.org/10.1006/nimg.2002.1136

Deichmann, R., Gottfried, J. A., Hutton, C., & Turner, R. (2003). Optimized EPI for fMRI studies of the orbitofrontal cortex. *NeuroImage*, *19*(2 Pt 1, 430–441. https://doi.org/10.1016/s1053-8119(03)00073-9

Eibenstein, A., Fioretti, A. B., Lena, C., Rosati, N., Ottaviano, I., & Fusetti, M. (2005). Olfactory screening test: Experience in 102 Italian subjects. *Acta Otorhinolaryngologica Italica: Organo Ufficiale Della Societa Italiana Di Otorinolaringologia E Chirurgia Cervico-Facciale*, *25*(1), 18–22.

Eliezer, M., Hamel, A.-L., Houdart, E., Herman, P., Housset, J., Jourdaine, C., … Hautefort, C. (2020). Loss of smell in patients with COVID-19: MRI data reveal a transient edema of the olfactory clefts. *Neurology*, *95*(23), e3145–e3152. https://doi.org/10.1212/WNL.0000000000010806

Fazekas, F., Chawluk, J. B., Alavi, A., Hurtig, H. I., & Zimmerman, R. A. (1987). MR signal abnormalities at 1.5 T in Alzheimer's dementia and normal aging. *American Journal of Roentgenology*, *149*(2), 351–356. https://doi.org/10.2214/ajr.149.2.351

Friston, K. J., Williams, S., Howard, R., Frackowiak, R. S., & Turner, R. (1996). Movement-related effects in fMRI time-series. *Magnetic Resonance in Medicine*, *35*(3), 346–355. https://doi.org/10.1002/mrm.1910350312

Fukushima, M., Betzel, R. F., He, Y., van den Heuvel, M. P., Zuo, X.-N., & Sporns, O. (2018). Structure-function relationships during segregated and integrated network states of human brain functional connectivity. *Brain Structure & Function*, *223*(3), 1091–1106. https://doi.org/10.1007/s00429-017-1539-3

Garrison, K. A., Scheinost, D., Finn, E. S., Shen, X., & Constable, R. T. (2015). The (in)stability of functional brain network measures across thresholds. *NeuroImage*, *118*, 651–661. https://doi.org/10.1016/j.neuroimage.2015.05.046

Goebel, R. (2012). BrainVoyager—Past, present, future. *NeuroImage*, *62*(2), 748–756. https://doi.org/10.1016/j.neuroimage.2012.01.083

Good, P. (2005). *Permutation, parametric and bootstrap tests of hypotheses*. New York, NY: Springer-Verlag. https://doi.org/10.1007/b138696

Groppe, D. M., Urbach, T. P., & Kutas, M. (2011). Mass univariate analysis of event-related brain potentials/fields I: A critical tutorial review. *Psychophysiology*, *48*(12), 1711–1725. https://doi.org/10.1111/j.1469-8986.2011.01273.x

Hagmann, P., Jonasson, L., Deffieux, T., Meuli, R., Thiran, J.-P., & Wedeen, V. J. (2006). Fibertract segmentation in position orientation space from high angular resolution diffusion MRI. *NeuroImage*, *32*(2), 665–675. https://doi.org/10.1016/j.neuroimage.2006.02.043

Han, P., Hummel, T., Raue, C., & Croy, I. (2019). Olfactory loss is associated with reduced hippocampal activation in response to emotional pictures. *NeuroImage*, *188*, 84–91. https://doi.org/10.1016/j.neuroimage.2018.12.004

Han, P., Zang, Y., Akshita, J., & Hummel, T. (2019). Magnetic resonance imaging of human olfactory dysfunction. *Brain Topography*, *32*(6), 987–997. https://doi.org/10.1007/s10548-019-00729-5

Hinz, A., Luck, T., Riedel-Heller, S. G., Herzberg, P. Y., Rolffs, C., Wirkner, K., & Engel, C. (2019). Olfactory dysfunction: Properties of the Sniffin' sticks screening 12 test and associations with quality of life. *European Archives of Oto-Rhino-Laryngology*, *276*(2), 389–395. https://doi.org/10.1007/s00405-018-5210-2

Hornuss, D., Lange, B., Schröter, N., Rieg, S., Kern, W. V., & Wagner, D. (2020). Anosmia in COVID-19 patients. *Clinical Microbiology and Infection*, *26*(10), 1426–1427. https://doi.org/10.1016/j.cmi.2020.05.017

Iadecola, C., Anrather, J., & Kamel, H. (2020). Effects of COVID-19 on the nervous system. *Cell*, *183*(1), 16–27.e1. https://doi.org/10.1016/j.cell.2020.08.028

Iravani, B., Peter, M. G., Arshamian, A., Olsson, M. J., Hummel, T., Kitzler, H. H., & Lundström, J. N. (2021). Acquired olfactory loss alters functional connectivity and morphology. *Scientific Reports*, *11*(1), 16422. https://doi.org/10.1038/s41598-021-95968-7

Jenkinson, M., Beckmann, C. F., Behrens, T. E. J., Woolrich, M. W., & Smith, S. M. (2012). FSL. *NeuroImage*, *62*(2), 782–790. https://doi.org/10.1016/j.neuroimage.2011.09.015

Kobal, G., Hummel, T., Sekinger, B., Barz, S., Roscher, S., & Wolf, S. (1996). 'Sniffin' sticks': Screening of olfactory performance. *Rhinology*, *34*(4), 222–226.

Koralnik, I. J., & Tyler, K. L. (2020). COVID-19: A global threat to the nervous system. *Annals of Neurology*, *88*(1), 1–11. https://doi.org/10.1002/ana.25807

Laurens, R. K. (2021). A permutation test (aka randomization test). MATLAB. https://github.com/lrkrol/permutationTest.

Le Bon, S.-D., Pisarski, N., Verbeke, J., Prunier, L., Cavelier, G., Thill, M.-P., … Horoi, M. (2021). Psychophysical evaluation of chemosensory functions 5 weeks after olfactory loss due to COVID-19: A prospective cohort study on 72 patients. *European Archives of Oto-Rhino-Laryngology*, *278*(1), 101–108. https://doi.org/10.1007/s00405-020-06267-2

Lechien, J. R., Chiesa-Estomba, C. M., De Siati, D. R., Horoi, M., Le Bon, S. D., Rodriguez, A., … Saussez, S. (2020). Olfactory and gustatory dysfunctions as a clinical presentation of mild-to-moderate forms of the coronavirus disease (COVID-19): A multicenter European study. *European Archives of Oto-Rhino-Laryngology*, *277*(8), 2251–2261. https://doi.org/10.1007/s00405-020-05965-1

Lu, Y., Li, X., Geng, D., Mei, N., Wu, P.-Y., Huang, C.-C., … Yin, B. (2020). Cerebral micro-structural changes in COVID-19 patients—An MRI-based 3-month follow-up study. *EClinicalMedicine*, *25*, 100484. https://doi.org/10.1016/j.eclinm.2020.100484

Meinhardt, J., Radke, J., Dittmayer, C., Franz, J., Thomas, C., Mothes, R., … Heppner, F. L. (2021). Olfactory transmucosal SARS-CoV-2 invasion as a port of central nervous system entry in individuals with COVID-19. *Nature Neuroscience*, *24*(2), 168–175. https://doi.org/10.1038/s41593-020-00758-5

Miller, R., & Englund, K. (2020). Clinical presentation and course of COVID-19. *Cleveland Clinic Journal of Medicine*, *87*(7), 384–388. https://doi.org/10.3949/ccjm.87a.ccc013

Niesen, M., Trotta, N., Noel, A., Coolen, T., Fayad, G., Leurkin-Sterk, G., … De Tiège, X. (2021). Structural and metabolic brain abnormalities in COVID-19 patients with sudden loss of smell. *European Journal of Nuclear Medicine and Molecular Imaging*, *48*, 1890–1901. https://doi.org/10.1007/s00259-020-05154-6

Parkes, L., Fulcher, B., Yücel, M., & Fornito, A. (2018). An evaluation of the efficacy, reliability, and sensitivity of motion correction strategies for resting-state functional MRI. *NeuroImage*, *171*, 415–436. https://doi.org/10.1016/j.neuroimage.2017.12.073

Paterson, R. W., Brown, R. L., Benjamin, L., Nortley, R., Wiethoff, S., Bharucha, T., … Zandi, M. S. (2020). The emerging spectrum of COVID-19 neurology: Clinical, radiological and laboratory findings. *Brain: A Journal of Neurology*, *143*(10), 3104–3120. https://doi.org/10.1093/brain/awaa240

Peter, M. G., Fransson, P., Mårtensson, G., Postma, E. M., Nordin, L. E., Westman, E., … Lundström, J. N. (2021). Normal olfactory functional connectivity despite lifelong absence of olfactory experiences. *Cerebral Cortex (New York, N.Y.: 1991)*, *31*(1), 159–168. https://doi.org/10.1093/cercor/bhaa217

Power, J. D., Mitra, A., Laumann, T. O., Snyder, A. Z., Schlaggar, B. L., & Petersen, S. E. (2014). Methods to detect, characterize, and remove motion artifact in resting state fMRI. *NeuroImage*, *84*, 320–341. https://doi.org/10.1016/j.neuroimage.2013.08.048

Roesch, M. R., Stalnaker, T. A., & Schoenbaum, G. (2006). Associative encoding in anterior Piriform cortex versus orbitofrontal cortex during odor discrimination and reversal learning. *Cerebral Cortex*, *17*(3), 643–652. https://doi.org/10.1093/cercor/bhk009

Rolls, E. T., Huang, C.-C., Lin, C.-P., Feng, J., & Joliot, M. (2020). Automated anatomical labelling atlas 3. *NeuroImage*, *206*, 116189. https://doi.org/10.1016/j.neuroimage.2019.116189

Rubinov, M., & Sporns, O. (2010). Complex network measures of brain connectivity: Uses and interpretations. *NeuroImage*, *52*(3), 1059–1069. https://doi.org/10.1016/j.neuroimage.2009.10.003

Santangelo, G., Siciliano, M., Pedone, R., Vitale, C., Falco, F., Bisogno, R., … Trojano, L. (2015). Normative data for the Montreal cognitive assessment in an Italian population sample. *Neurological Sciences: Official Journal of the Italian Neurological Society and of the Italian Society of Clinical Neurophysiology*, *36*(4), 585–591. https://doi.org/10.1007/s10072-014-1995-y

Satterthwaite, T. D., Elliott, M. A., Gerraty, R. T., Ruparel, K., Loughead, J., Calkins, M. E., … Wolf, D. H. (2013). An improved framework for confound regression and filtering for control of motion artifact in the preprocessing of resting-state functional connectivity data. *NeuroImage*, *64*, 240–256. https://doi.org/10.1016/j.neuroimage.2012.08.052

Satterthwaite, T. D., Wolf, D. H., Loughead, J., Ruparel, K., Elliott, M. A., Hakonarson, H., … Gur, R. E. (2012). Impact of in-scanner head motion on multiple measures of functional connectivity: Relevance for studies of neurodevelopment in youth. *NeuroImage*, *60*(1), 623–632. https://doi.org/10.1016/j.neuroimage.2011.12.063

Satterthwaite, T. D., Wolf, D. H., Ruparel, K., Erus, G., Elliott, M. A., Eickhoff, S. B., … Gur, R. C. (2013). Heterogeneous impact of motion on fundamental patterns of developmental changes in functional connectivity during youth. *NeuroImage*, *83*, 45–57. https://doi.org/10.1016/j.neuroimage.2013.06.045

Schwarz, A. J., & McGonigle, J. (2011). Negative edges and soft thresholding in complex network analysis of resting state functional connectivity data. *NeuroImage*, *55*(3), 1132–1146. https://doi.org/10.1016/j.neuroimage.2010.12.047

Sedaghat, A. R., Gengler, I., & Speth, M. M. (2020). Olfactory dysfunction: A highly prevalent symptom of COVID-19 with public health significance. *Otolaryngology—Head and Neck Surgery: Official Journal of American Academy of Otolaryngology-Head and Neck Surgery*, *163*(1), 12–15. https://doi.org/10.1177/0194599820926464

Seubert, J., Freiherr, J., Djordjevic, J., & Lundström, J. N. (2013). Statistical localization of human olfactory cortex. *NeuroImage*, *66*, 333–342. https://doi.org/10.1016/j.neuroimage.2012.10.030

Sporns, O. (2018). Graph theory methods: Applications in brain networks. *Dialogues in Clinical Neuroscience*, *20*(2), 111–120. https://doi.org/10.31887/DCNS.2018.20.2/osporns

Stern, Y. (2002). What is cognitive reserve? Theory and research application of the reserve concept. *Journal of the International Neuropsychological Society*. *8*, 448–460. https://doi.org/10.7916/D8TQ7D3P

Theisen, F., Leda, R., Pozorski, V., Oh, J. M., Adluru, N., Wong, R., … Gallagher, C. L. (2017). Evaluation of striatonigral connectivity using probabilistic tractography in Parkinson's disease. *NeuroImage: Clinical*, *16*, 557–563. https://doi.org/10.1016/j.nicl.2017.09.009

Tobia, M. J., Yang, Q. X., & Karunanayaka, P. (2016). Intrinsic intranasal chemosensory brain networks shown by resting-state functional MRI. *Neuroreport*, *27*(7), 527–531. https://doi.org/10.1097/WNR.0000000000000579

Tschentscher, N., Ruisinger, A., Blank, H., Díaz, B., & von Kriegstein, K. (2019). Reduced structural connectivity between left auditory thalamus and the motion-sensitive planum temporale in developmental dyslexia. *The Journal of Neuroscience*, *1435–18*, 1435–1418. https://doi.org/10.1523/JNEUROSCI.1435-18.2018

Tzourio-Mazoyer, N., Landeau, B., Papathanassiou, D., Crivello, F., Etard, O., Delcroix, N., … Joliot, M. (2002). Automated anatomical labeling of activations in SPM using a macroscopic anatomical parcellation of the MNI MRI single-subject brain. *NeuroImage*, *15*(1), 273–289. https://doi.org/10.1006/nimg.2001.0978

van den Heuvel, M. P., de Lange, S. C., Zalesky, A., Seguin, C., Yeo, B. T. T., & Schmidt, R. (2017). Proportional thresholding in resting-state fMRI functional connectivity networks and consequences for patient-control connectome studies: Issues and recommendations. *NeuroImage*, *152*, 437–449. https://doi.org/10.1016/j.neuroimage.2017.02.005

Wahlund, L. O., Barkhof, F., Fazekas, F., Bronge, L., Augustin, M., Sjögren, M., … European Task Force on Age-Related White Matter Changes. (2001). A new rating scale for age-related white matter changes applicable to MRI and CT. *Stroke*, *32*(6), 1318–1322. https://doi.org/10.1161/01.str.32.6.1318

Weiss, T., Soroka, T., Gorodisky, L., Shushan, S., Snitz, K., Weissgross, R., … Sobel, N. (2020). Human olfaction without apparent olfactory bulbs. *Neuron*, *105*(1), 35–45.e5. https://doi.org/10.1016/j.neuron.2019.10.006

World Health Organization. (2020). *Clinical management of COVID-19: Living guidance*, May 27, 2020. World Health Organization. Available from https://www.who.int/publications-detail-redirect/clinical-management-of-covid-19

Xia, M., Wang, J., & He, Y. (2013). BrainNet viewer: A network visualization tool for human brain connectomics. *PLoS One*, *8*(7), e68910. https://doi.org/10.1371/journal.pone.0068910

How to cite this article: Esposito, F., Cirillo, M., De Micco, R., Caiazzo, G., Siciliano, M., Russo, A. G., Monari, C., Coppola, N., Tedeschi, G., & Tessitore, A. (2022). Olfactory loss and brain connectivity after COVID-19. *Human Brain Mapping*, *43*(5), 1548–1560. https://doi.org/10.1002/hbm.25741